Forest Ecology and Management 594 (2025) 122948

Contents lists available at ScienceDirect

Forest Ecology and Management

journal homepage: www.elsevier.com/locate/foreco

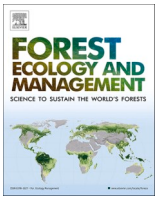

Riparian field elm (*Ulmus minor*) is sensitive to drought, and fast-growing trees are susceptible to Dutch elm disease

J. Julio Camarero [a,*], Antonio Gazol [a], Ángel Fernández-Cortés [b,c], Michele Colangelo [d]

[a] Instituto Pirenaico de Ecología (IPE-CSIC), Avda. Montañana 1005, Zaragoza 50192, Spain
[b] Departamento de Biología y Geología, Universidad de Almería, Almería 04120, Spain
[c] Centro Andaluz para el Cambio Global "Hermelindo Castro" (ENGLOBA), Universidad de Almería, Almería, Spain
[d] Dipartimento di Scienze Agrarie, Forestali, Alimentari ed Ambientali, Università degli Studi della Basilicata, Potenza 85100, Italy

ARTICLE INFO

Keywords:
Dendroecology
Earlywood anatomy
Floodplain forest
Ulmus minor

ABSTRACT

Dutch elm disease (DED) is decimating field elm (*Ulmus minor*) populations in Europe. The species is subjected to periodic DED outbreaks leading to a loss of vigor (canopy dieback, radial growth, mortality rate), but drought could also stress these riparian stands and interact with DED. However, we lack a quantitative characterization on the impacts of DED and drought on the vigor of elm populations. To assess how river geomorphology, growth rate and intrinsic water-use efficiency (iWUE) influence elm vulnerability to DED, we measured tree-ring, wood anatomy and $\delta^{13}C$ in non-declining (ND) and declining (D) trees in an urban site. We also assessed the elm vigor status in 13 elm stands experiencing different geomorphological (river sinuosity index) and stand structural features along the middle Ebro basin (North Eastern Spain). Tree-ring and wood-anatomy series were correlated with climate variables (temperature, precipitation), a drought index and river flow data. Elm was more abundant at sites with lower river sinuosity and where *Populus alba* was abundant. On average, 64 ± 12 % (mean ± SE) of the elm basal area corresponded to dead trees. The probability of death was above 50 % for elms with diameter > 21 cm. Dry-warm conditions from the prior to the current summer and low spring river flow decreased elm growth. During the severe drought of 2012, the mean ring width was 36 % lower than the long-term average (2.74 mm). However, elm showed a rapid post-drought growth recovery. The earlywood diameter decreased in response to warm conditions in the previous winter. D trees grew more in the past and showed higher iWUE than ND trees. Our findings contribute to better knowledge of declining elms by showing their vulnerability to drought, and how fast-growing elm trees are prone to DED damage.

1. Introduction

Riparian and floodplain forests are among the most dynamic and threatened terrestrial ecosystems (Dufour and Piégay, 2008, Stella and Bendix, 2019). The dynamics of riparian forests makes them responsive to several stressors including changes in hydrologic regimes (e.g., river regulation, groundwater depletion) and extreme climate events (e.g., droughts, floods) (Rodríguez-González et al., 2010). Changes in these stressors occur at different spatial and temporal scales (Havrdová et al. 2023). Therefore, restoration and conservation programs of riparian forests should explicitly consider long-term river-forest interactions to encompass historical hydrological and climatic variability (Gurnell et al., 2020; Janssen et al., 2021, Camarero et al., 2023b).

Long-term groundwater decline due to river regulation and short-term drought stress can trigger the growth decline of some riparian forests and tree species, particularly in semiarid regions (Stromberg et al., 1996; Williams and Cooper, 2005). Several riparian *Populus* and *Fraxinus* species have shown a high vulnerability to hydrological droughts and heat waves triggering growth declines and massive dieback and mortality events (Rodríguez-González et al., 2021; Moran et al., 2023). Therefore, historical reconstructions of tree growth combined with complementary proxies of theoretical hydraulic conductivity (wood anatomy) and intrinsic water-use efficiency –iWUE–, inferred from wood C isotope discrimination data ($\delta^{13}C$), are required to understand how menaced riparian forests respond to interacting abiotic and biotic stressors. These proxies allowed to gather information on

* Corresponding author.
E-mail addresses: jjcamarero@ipe.csic.es (J.J. Camarero), agazol@ipe.csic.es (A. Gazol), acortes@ual.es (Á. Fernández-Cortés), michele.colangelo@unibas.it (M. Colangelo).

https://doi.org/10.1016/j.foreco.2025.122948
Received 7 February 2025; Received in revised form 21 June 2025; Accepted 24 June 2025
Available online 28 June 2025

riparian tree functioning and vulnerability to abiotic and biotic stressors such as droughts and pathogens, respectively (e.g. Camarero et al., 2023a). Here, we hypothesize that hydrological constraints may contribute to vulnerability of riparian tree species and predispose to pathogen-induced mortality. Specifically, we focus on the interactions between drought and Dutch elm disease (DED) on field elm (*Ulmus minor*) populations.

In addition to abiotic factors, biotic stressors including invasive species and pathogens threaten several riparian tree species (*Ulmus*, *Fraxinus*, and *Alnus* spp.) and contribute to their decline (e.g. Colangelo et al., 2018, Valor et al., 2020). A paradigmatic example is the DED, caused by the fungi *Ophiostoma ulmi* and *Ophiostoma novo-ulmi*. These fungi species block the xylem vessels of elms (*Ulmus* spp.) causing crown wilting, canopy dieback and tree death (Brasier, 1991, 2000). Therefore, DED-induced xylem blockage could intensify the drought vulnerability of riparian elm populations. Among the most susceptible species to DED is the field elm, a riparian, winter-deciduous tree widely distributed across riparian forests of southern Europe (Caudullo and De Rigo, 2016). This elm species has great ecological and cultural importance in Europe, but it has been decimated by DED during the 20th century reducing its abundance in many regions, and promoting its transformation from a tall to a small resprouting tree (Mittempergher, 1989). Recurrent DED cycles affect trees once they reach a size vulnerability threshold such as 3–10 m in height (Martín et al., 2023). DED is very aggressive and is transmitted by bark beetles (*Scolytus* spp.), which disperse the fungi spores among trees, or throughout root grafts, attacking primarily mature trees and killing them in 2 −3 years (Mittempergher and Santini, 2004).

The DED pandemic lead to a severe demographic decline of field elm, thus facilitating the expansion of the DED-resistant Siberian elm (*Ulmus pumila* L.) (Bertolasi et al., 2015). The field elm forms ring-porous wood that allows rapid uptake of water and nutrients and higher growth rates (Ellmore and Ewers, 1985). The formation of wider earlywood vessels in field elm enhances water transport but also facilitates pathogen spread, making this species susceptible to DED damage through xylem cavitation (Solla et al., 2005). To restore field elm populations, DED-resistant genotypes were developed, but they showed different susceptibility to abiotic stressors such as drought and waterlogging (Martínez-Arias et al., 2020). Furthermore, drought can contribute to tree death when combined with phloem girdling by bark beetles (Martín et al., 2023). Even if DED is the ultimate cause of tree death, better knowledge on how hydrological and climatic droughts contribute to the long-term decline in field elm growth is lacking (e.g. Tulik et al., 2020, Kibler et al., 2021; Schmucker et al., 2023). We aim to answer how do river geomorphology and tree vigor influence elm abundance and DED impacts, respectively. Tree vigor is defined based on tree radial growth rate and death probability related to DED impacts including canopy dieback. For instance, it could be expected that well-preserved elm stands would appear at sites with higher soil moisture and river sinuosity, whereas riparian elm forests in sites with low river sinuosity would be more impacted by drought stress and DED. In addition, fast-growing trees reaching a lethal diameter threshold would be prone to DED-triggered death.

Here, we propose using radial growth, wood anatomy and $\delta^{13}C$ data to retrospectively characterize hydrology, drought and DED impacts on elm vigor. The objectives of this study are: (i) to describe the site geomorphology, structure and vigor status of field elm stands across the middle Ebro Basin, North Eastern Spain, where the species has been severely affected by DED, (ii) to assess climate- and streamflow-growth relationships and infer the main climatic constraints of growth based on dendrometer data, and (iii) to measure recent changes in growth and $\delta^{13}C$ of living trees and dying trees with DED symptoms. To achieve these objectives, we estimated the river sinuosity and sampled 13 elm stands classifying 180 trees as dead or alive (objective (i)), we quantified growth rates in 108 trees from 6 sites, including two urban stands located in Zaragoza city (objective (ii)), we measured intra-annual growth changes using dendrometers and wood anatomy in selected well-preserved stands, i.e. not disturbed by local anthropogenic activities (objective (ii)), and we compared growth rates and wood $\delta^{13}C$ in coexisting trees showing or not showing DED symptoms in the two urban stands (objective (iii)). We expect that: (i) elm mortality linked to DED will be widespread and related to a size threshold, (ii) elm growth will be highly dependent on moisture conditions in spring, when growth rates should peak, and (iii) DED will lead to an abrupt growth decline and an increase of $\delta^{13}C$ in DED-symptomatic trees due to xylem blocking and branch dieback.

2. Material and methods

2.1. Study sites

We selected 13 mature riparian forests ("soto" in Spanish) located in the Middle Ebro basin, north-eastern Spain (Fig. 1, Table 1). The study area is characterized by a low longitudinal slope and the Ebro river forms meandering channels (Ollero, 1990, 2007). Site selection was based on a previous extensive sampling of riparian forests in this area considering diverse geomorphological and structural conditions (Camarero et al., 2023b). Site selection followed two criteria: (i) some sampled sites were mature riparian forests with old and large trees and elevated diversity (e.g., Soto de la Duquesa), and (ii) others were located in urban areas (Zaragoza city) and showed low structural diversity (e.g., Puente de Hierro). This ample gradient of forest types subjected to different hydrological conditions and with different elm abundance allowed to assess the impacts of different geomorphological, hydrological, climatic and structural conditions on tree vigor and DED impacts.

The Ebro basin occupies 85,362 km^2 and is the third largest hydrographic basin in the Mediterranean basin. This river was regulated through the building of dams and dikes in the 1950s and 1960s (Frutos et al., 2004). Therefore, the ecohydrological dynamics of the study sites are very different with some sites presenting dykes and altered flow (e.g., Soto de Partinchas; Fig. S1). Other sites are more structurally diverse and present free-flowing river dynamics (e.g., Soto de la Duquesa, Soto de la Remonta) (Ayerra, 1988). In short, structurally diverse with free-flowing river dynamics and the ones with dykes and altered flow, located near Zaragoza city, are studied.

In the study sites, river flow peaks from January to April (Fig. S2), when the highest soil moisture is recorded, and precipitation peaks in spring and autumn. According to data from a gauging station located near Tudela town (Castejón station, 1° 41' W, 42° 11' N, 260 m a.s.l.; period 1970–2018) the average annual discharge of the Ebro river registered was 7177 hm^3 and the contributing area of the catchment upstream the gauge station was 25,194 km^2. Downstream, near Zaragoza city, where there is another gauging station, the water table depth showed maximum values from October to April and minimum values from May to September (Camarero et al., 2023b). Recent periods with very low (close to the mean – 1.96 SD) river discharge or flow values from winter to spring were: 1988–1990, 2001–2002, 2011–2012 and 2016–2017 (Fig. S2).

In the study area, the climate is semi-arid continental Mediterranean with annual precipitation ranging 350–470 mm. Therefore, the study sites are located near the xeric distribution limit of the species in Spain (Fig. 1). The coldest and warmest months are January (5.4–5.6 °C) and July (22.7–23.6 °C), respectively. The summer drought lasts from June to September. In this region, marl and gypsum deposits abound leading to the formation of loamy-sandy or loamy-silty soils. Soils are basic (pH = 8.2) and relatively fertile (N = 0.61 %, C/N = 18.6).

The study riparian forests are dominated by tamarisks (*Tamarix* spp.), white willow (*Salix alba* L.) and black poplar (*Populus nigra* L.) near the river bank, silver poplar (*Populus alba* L.) in the transition zone, and narrow-leaved ash (*Fraxinus angustifolia* Vahl.) with scattered elm trees (*Ulmus minor* Mill.) located inland. Vines are also observed (*Hedera helix* L.) with high cover values in DED-affected stands or in gaps (Fig. S3). We also detected scars in some stems caused by the Eurasian

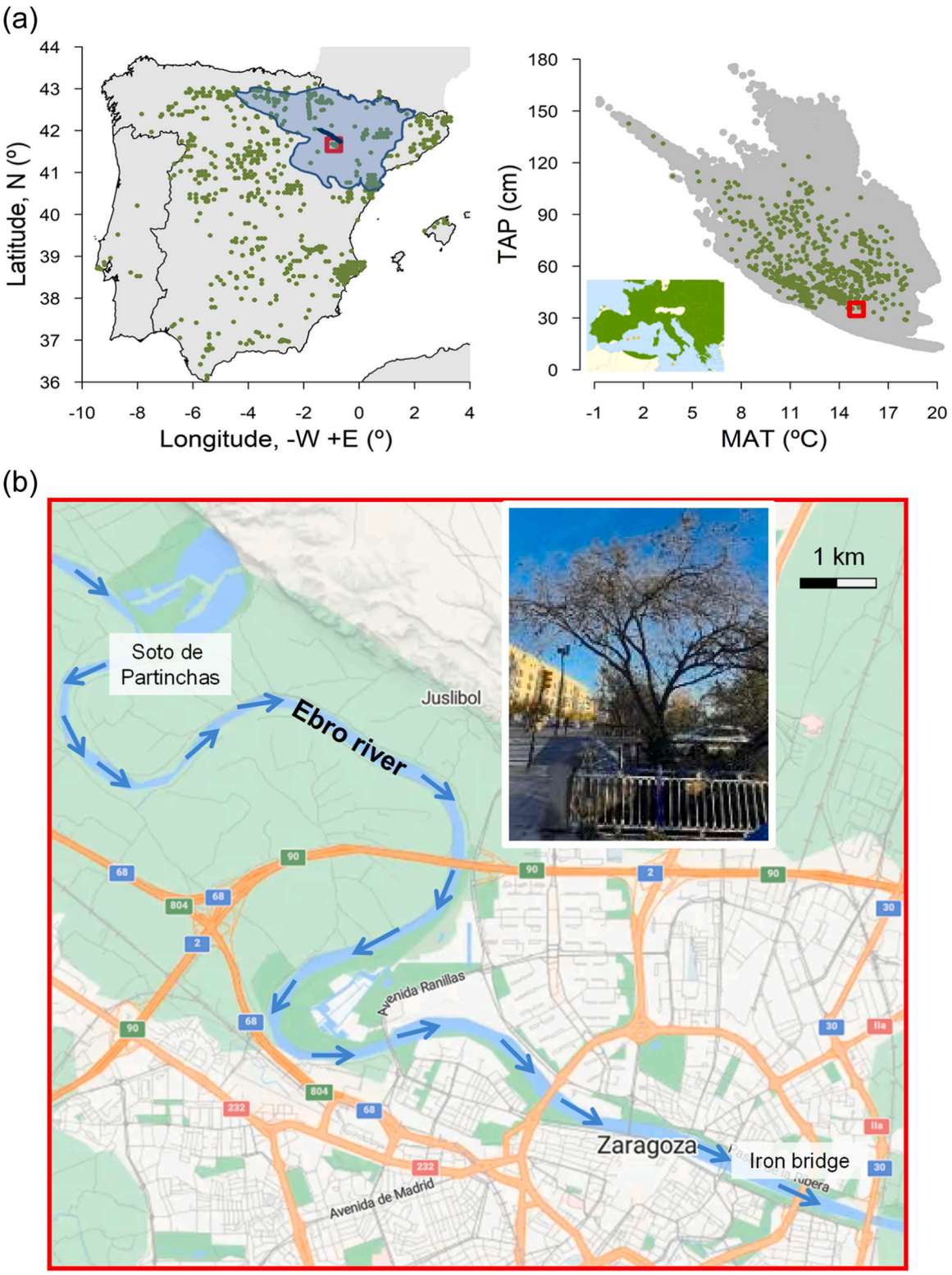

Fig. 1. Sampling locations of elm stands along the Middle Ebro Basin in North Eastern Spain. In plot (a), the approximate area of the Ebro Basin (blue area), the sampled stretch of the middle Ebro River and the location of Zaragoza city (red square) are indicated. The situation of Zaragoza across the elm bioclimatic distribution (MAT is mean annual temperature; TAP is the total annual precipitation) is also indicated. The small map shows the elm distribution in Europe. In plot (b) the locations of the two sites sampled in Zaragoza city (well-preserved "Soto de Partinchas" site, urban "Iron bridge" site) are also indicated. The image corresponds to a dying elm tree sampled near the Iron bridge site.

Table 1
River sinuosity and structural variables (basal area, stem density and importance values) calculated for elm and the main coexisting tree species in riparian forests sampled along the middle Ebro basin. Note that basal area and density refer to all tree species. Bold values indicate sites with elm importance values > 0.10. Basal area and stem density are reported only for living trees with data on basal area of dead elm trees presented in Fig. 2 (see the correspondence between site number and name in that figure). Higher and lower values of the river sinuosity index indicate more meandering (curved) or straight river channels, respectively.

Site number	Site name	River side	No. sampled transects	Sinuosity index	Basal area (m^2 ha^{-1})	Stem density (stem ha^{-1})	Importance values					
							Ulmus minor	*Populus alba*	*Populus nigra*	*Fraxinus angustifolia*	*Tamarix* spp.	*Salix alba*
1	Soto del Hormiguero	Right	1	1.442	40.4	1550	0.00	0.00	0.65	0.00	0.00	0.35
2	Soto de la Duquesa	Left	2	1.060	115.8	1475	**0.17**	0.44	0.38	0.16	0.01	0.00
3	Soto del Estajao	Right	1	1.254	117.2	1050	0.02	0.18	0.34	0.02	0.00	0.44
4	Soto de Giraldelli	Right	1	1.298	74.4	900	0.00	0.00	0.66	0.06	0.00	0.29
5	Soto de la Remonta	Right	3	1.067	56.0	900	**0.37**	0.47	0.89	0.16	0.00	0.03
6	Murillo de las Limas	Left	1	1.190	43.3	1050	**0.51**	0.42	0.00	0.00	0.07	0.00
7	Quebrado, El Ramillo y la Mejana	Left	1	1.082	49.1	1050	0.00	0.20	0.00	0.37	0.28	0.14
8	Soto de Novillas	Right	1	1.093	58.8	2000	0.10	0.42	0.00	0.29	0.09	0.00
9	Soto de la Alameda	Right	1	1.289	53.6	1500	0.00	0.00	0.00	0.00	0.57	0.43
10	Soto de Partinchas	Left	3	1.155	63.2	1933	**0.32**	0.46	0.09	0.16	0.17	0.76
11	Puente de Hierro[#]	Right	2	1.082	37.5	710	**0.35**	0.50	0.00	0.00	0.00	0.00
12	La Mejana de Pastriz	Left	2	1.260	65.9	825	0.10	0.49	0.07	0.07	0.04	0.00
13	Soto de Nís	Right	1	1.156	22.2	950	0.00	0.00	0.00	0.35	0.25	0.00

[#]Iron bridge.

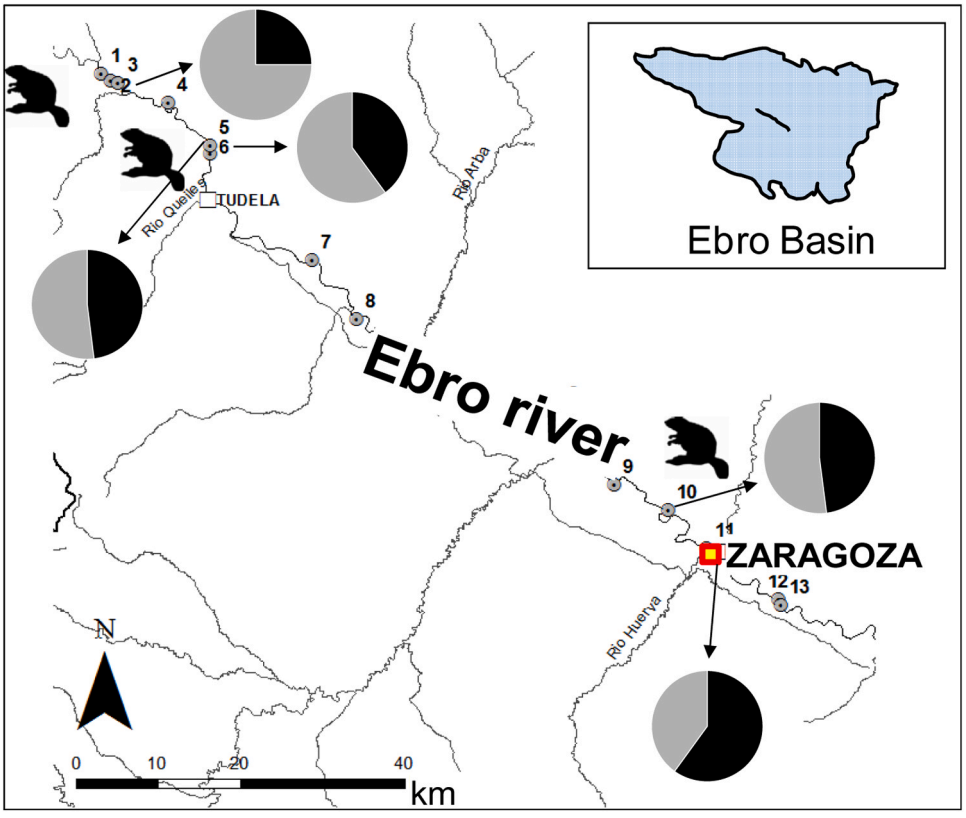

Fig. 2. Elm mortality in the sites studied across the middle Ebro basin where elm abundance was high (importance value > 0.10). The black sections of the pie charts show the basal area of dead elm trees (%) measured in the sampled stands while the grey area shows the basal area of living trees (%). Studied sites are indicated with numbers and the red square indicates the "Soto de Partinchas" site. Beaver silhouettes indicate the presence of beaver feeding marks in stems. The inset shows the river section (dark blue segment) studied in the Ebro basin (North Eastern Spain). See more data in Table 1.

beaver (*Castor fiber* L.) foraging activity (Fig. 2). This species was re-introduced in the study region in the 1990s and it is rapidly expanding.

2.2. Climate data, drought indices, river flow and sinuosity

Due to the lack of long and homogeneous climate records for the study area, we used 0.1°-gridded monthly climate data (mean maximum and minimum temperatures, total precipitation) corresponding to the E-OBS climate dataset version 28.0e (Cornes et al., 2018).

To assess changes in drought severity and duration we used Standardized Precipitation Evapotranspiration Index (SPEI) monthly and weekly data gridded at 0.5º and 1.1 km^2 resolutions, respectively. These data were downloaded from the Global Drought Monitor (http://spei.csic.es/index.html) and the Spanish Drought Monitor (https://monitordesequia.csic.es/) websites, respectively. The SPEI is a multi-scalar drought index calculated on cumulative climate water balances which depend on temperature and precipitation (Vicente-Serrano et al., 2010). We considered SPEI values calculated at 1-, 3-, 6-, 9- and 12-month long scales.

Monthly river flow data were obtained from the Castejón and Zaragoza (0º 53' W, 41º 40' N, 201 m a.s.l.; period 1913–2021) gauging stations located at 9 and 6.5 km, respectively, upstream from some of the best preserved study sites (Soto de la Remonta, Soto de Partinchas). They were converted into water-year data by summing monthly values. These data are available from the Spanish National Flow and Discharge Database (Centro de Estudios y Experimentación de Obras Públicas, data available at https://ceh.cedex.es).

To characterize the recent dynamics of the Ebro river near the study sites we analysed aerial photographs (taken in 1956 and 2014–2015) and calculated the hydraulic sinuosity index (Mueller, 1968), i.e. the ratio between the curvilinear and the Euclidean distances between the end points of the channel. This index was used as a proxy of river dynamics with higher and lower values indicating more curved or straight river channels, respectively. The images were analysed with ArcGis ver. 10.0 (ESRI, Redlands, USA) and considering 4000-m long segments. The river channel was digitized at scale 1:10000 following the axis of the main Ebro wet channel over digital ortho-photographs for the study periods (see more details in Camarero et al., 2023b).

2.3. Field sampling and dendrometer data

In the 13 sites, we selected representative stands and located from one to three 50-m long transects per site depending on the stand size (Table 1). The position and elevation of the start (0 m) and end (50 m) of each transect were recorded using a GPS (resolution ± 5 m). The transects were oriented perpendicular to the flow direction along the topographic gradient. Then, the distance and diameters at breast height (dbh, measured at 1.3 m) of the four closest neighbouring trees located in four different quadrants were measured every 2 m along the transect, also annotating the species identity and vigor (dead or living tree).

In total, 20 transects and 2080 quadrants were measured. These data were used to estimate the basal area and the stem density of each tree species using the point-quarter method (Cottam and Curtis, 1956). The importance value of each tree species in each site was obtained as the average of the relative density and basal area values of each tree species within each of the measured transects (Muller-Dombois and Ellenberg, 1974).

Lastly, two cores were extracted at 1.3 m using a 5-mm Pressler increment borer (Haglöf, Sweden) from 10 to 27 elm trees sampled in each of the six selected stands (Table 2). In the case of the urban "Iron bridge - left margin" site, we sampled 10 additional DED-affected trees (D, declining trees) and 10 asymptomatic trees (ND, non-declining trees to compare their recent growth trends.

Dendrometers were used to determine during which period tree water deficit occurs. To measure inter- and intra-annual changes in stem radius, we installed five point dendrometers (TOMST, Prague, Czech Republic) in five apparently healthy elm trees located in the Soto de Partinchas site. Regrettably, living but DED- affected trees were rare in this site, and we could not install enough dendrometers on them. The dendrometers were installed at 3 −4 m height to avoid vandalism or robbery after carefully removing the dead bark. We also installed three soil moisture sensors (TMS-4, TOMST, Prague, Czech Republic), near the study sites to measure moisture at 15-cm depth; however, data were only available for 2023 because they were stolen in 2024. In all cases, measurements were taken every 15 min. The point dendrometers have a resolution of 0.27 μm and a span of 8890 μm (see https://tomst.com/web/en/systems/tms/point-dendrometer/). From January to September, the mean maximum and minimum temperatures were 24.8 and 12.7 ° C and 24.3 and 12.4 ° C in 2023 and 2024 (Fig. S4), respectively, whereas the accumulated precipitation values were 188 and 250 mm (data from Zaraporta Airpot station, 41.667º N, 1.023º W, 251 m a.s.l.; located at 7.3 km from the Soto de Partinchas study site).

To process the dendrometer data we applied the zero-growth concept (Zweifel et al., 2016). Changes in stem radius were separated into growth (irreversible stem increment) and tree water deficit (reversible stem swelling and shrinking) components. Growth is considered to occur when the cumulative radial increment increases and exceeds its previous maximum value. The processing of dendrometer data was done using the R-package treenetproc (Knüsel et al., 2021). Dendrometer data were standardized using mean daily shrinkage. Daily measures of growth and tree water deficit were averaged for the five individuals at a monthly scale to visualize seasonal patterns. In addition, the growth rate (μm day^{-1}) was calculated as the amount of growth per day and averaged at the monthly scale. The metrics were calculated for the 2023 and 2024 years to interpret their patterns separately.

2.4. Tree-ring data

Wood samples were processed using dendrochronology (Fritts, 1976) to assess the impacts of river flow, climate conditions, drought severity, and DED on tree radial growth. First, the wood samples were air-dried, and then cross-sections were cut using a sledge microtome (Gärtner and Nievergelt, 2010). Samples were visually cross-dated under the binocular scope and scanned at 1200 dpi (Epson Expression 10000XL). Tree-ring widths were measured with a 0.001 mm resolution along two radii per tree using the CooRecorder software (Larsson and Larsson, 2018). The visual cross-dating was checked using the COFECHA software, which calculates moving correlations between the individual series and the mean site series (Holmes, 1983). Tree age at 1.3 m was estimated by counting the number of rings along the oldest core of each

Table 2
Tree-ring width data and statistics. No trees and No. radii is the number of measured trees and cores, respectively. TRW is the mean tree-ring width, SD is the standard deviation, AR1 is the first-order autocorrelation, MS is the mean sensitivity, and rbar is the mean correlation between individual ring-width series.

Site (code)	No trees	No radii	Time span	Age (years)	TRW (mm)	SD (mm)	AR1	MS	rbar
Soto de la Duquesa (DU)	11	22	1962 −2019	30 ± 5	2.67	1.51	0.71	0.33	0.28
Murillo de Limas (ML)	27	54	1921 −2019	65 ± 5	2.18	1.27	0.65	0.32	0.31
Soto de la Remonta (RE)	15	29	1921 −2019	67 ± 3	1.83	1.28	0.82	0.23	0.51
Soto de Partinchas (PA)	20	39	1953 −2019	37 ± 4	2.28	1.34	0.48	0.42	0.34
Iron bridge - left margin (IB-L)	20	38	1981 −2019	22 ± 2	4.53	2.14	0.42	0.34	0.39
Iron bridge - right margin (IB-R)	15	28	1976 −2019	26 ± 3	2.94	1.42	0.38	0.40	0.36

tree whenever it reached the pith or presented curved, innermost rings. In the ND and D trees sampled in the "Iron bride – left margin" site, tree-ring width data were converted into basal area increment (BAI) to better assess and compare the growth trends of the two vigor classes. We calculated BAI only in this site because trees were very young and this helped to better detect growth divergences between D and ND trees.

To calculate climate-, drought- or flow-growth relationships, the individual ring-width series were converted into indexed ring-width series through standardization and detrending (Fritts, 1976). These procedures allow for the removal of size-related trends in growth and emphasize high-frequency variability. We fitted negative linear or exponential functions to individual ring-width series and obtained width indices by dividing the observed by the fitted values. Then, autoregressive models were fitted to remove the first-order autocorrelation of the series of dimensionless indices. The resulting pre-whitened individual series were averaged using a bi-weight robust mean to obtain mean residual ring-width series for each site (Fritts, 1976). To summarize the characteristics of each ring-width sites series, several statistics were calculated (cf. Briffa and Jones, 1990) including: the mean and standard deviation (SD) of ring widths, the first-order autocorrelation (AR1), the mean sensitivity of ring-width indices (MS), which measures the relative changes in width between consecutive rings, and the mean correlation of the individual indexed series (rbar). These procedures were done using the dplR package (Bunn, 2008, 2010; Bunn et al., 2024) in the R statistical software (R Core Team., 2024).

To assess the dependence between site series of ring-width indices, i.e. the similarity in year-to-year growth variability among sites, first we calculated Pearson correlations considering the common and best-replicated period 1981–2019 (Table S1). Then, a Principal Component Analysis (PCA) was performed on the covariance matrix of the chronologies for the same period. The first (PC1) and second (PC2) principal components were kept because they accounted for more than 70 % of the total variability. The PCA was calculated using the vegan R package (Oksanen et al., 2025).

2.5. Earlywood anatomy data

To assess how river flow, climate conditions and drought severity impacted on theoretical hydraulic conductivity, we measured earlywood anatomy in five elm trees sampled in two well-preserved sites (Soto de la Remonta, Soto de Partinchas). We selected trees whose ring-width series were significantly ($p < 0.05$) and positively correlated with the mean series of the species in the site. We only measured earlywood vessels as this wood type accounts for most of the hydraulic conductivity (ca. 90 %) in elm (Ellmore and Ewers, 1985). To measure earlywood anatomical variables we followed Camarero et al. (2021, 2023a). We took an additional 5-mm diameter core per tree and the surface of the cores was transversally cut using a sledge microtome. Then, transversal, 15– to 20 μm thick wood sections were prepared from each core by dividing it into 2-cm long pieces. Samples were stained with safranin (1 %) and astra blue (2 %) and images were captured at 20–40x magnification using a light microscope (Olympus BH2). Earlywood vessels were considered those with lumen diameters larger than 30 μm (Ellmore and Ewers, 1985) located in the first half of the ring (Table 3, Fig. S5). We measured each vessel transversal area and converted into radial vessel diameters assuming a circular shape. Vessels were measured in a window of 4 mm (core width) along the common period 1980–2011 using the ImageJ software (Schneider et al., 2012). After measuring the diameter of all earlywood vessels (d) we calculated: the vessel density, the maximum vessel diameter and the hydraulic diameter (Dh), as they impact hydraulic conductivity and xylem vulnerability to cavitation. The Dh was calculated following Sperry et al. (1994):

$$Dh = (\sum d^5 / d^4) \quad (1)$$

To calculate climate- or flow-anatomy relationships, the series of earlywood anatomical variables were also detrended and standardized as ring-width series.

2.6. Wood $\delta^{13}C$ analyses

To assess how DED impacted on tree iWUE, wood $\delta^{13}C$ measurements were carried out. Groups of annual tree rings were separated under the binocular using scalpels. This was done for five ND trees and five D trees from the "Iron bridge – left margin" site and considering the periods 2011 −2014 and 2021 −2024, i.e. during and after the severe 2012 drought. Wood samples were milled and homogenised using a ball mill (Retsch MM301, Haan, Germany). Wood aliquots (0.8–1.2 mg) were weighed on a microbalance (AX205 Mettler Toledo, OH, USA) into tin foil capsules.

Isotope analyses were carried out at the Stable Isotope Laboratory of the University of Almería (Spain). Encapsulated wood samples were combusted to CO_2 at a combustion module coupled to a cavity ring-down spectroscopy (CRDS) Ssstem (G2201-I Analyzer, Picarro). The released CO_2 was transferred to a Picarro Liaison A0301 interface and inputted into CRDS for analysis. The $\delta^{13}C$ values were referenced to the Vienna PeeDee Belemnite (V-PDB) scale. USGS (USGS-40 l-Glutamic acid) and IAEA standards (IAEA-603 and NBS-18 calcites) were used to calibrate the CM-CRDS system, and sugarcane, acetanilide, and urea were used as working reference standards for consecutive $\delta^{13}C$ analyses of the wood samples. Based on analyses of the standards, precision and accuracy 0.09 – 0.26 ‰ and −0.87 – 0.03 ‰ (n = 9), respectively.

2.7. Statistical analyses

Several variables (tree diameter, mean ring widths, correlation between individual ring-width series, wood $\delta^{13}C$) were compared between the two intensively studied sites using t tests after log-transforming to achieve normality. Spearman correlations (r_s) between importance values and river sinuosity were calculated (objective (i)).

To estimate a size threshold of DED-induced mortality (objective (i)), a generalized linear model based on a binomial distribution of elm death probability as a function of diameter (dbh) was fitted (n = 180 trees). This was done using the glm function in the R software (R Core Team., 2024).

To assess growth or wood anatomy responses to climate variability, river flow and drought severity (objective (ii)), Pearson correlations were calculated between series of ring-width indices and monthly climate variables (mean maximum and minimum temperatures, precipitation, soil moisture), river flow data, or drought indices (SPEI). This was done using the treeclim R Package (Zang and Biondi, 2015). The climate window of these analyses spanned from the prior to the current September. All analyses were carried out in the R statistical software (R Core Team., 2024).

Table 3
Earlywood anatomy data measured in elm trees of two selected sites (period 1981 −2019). Different letters indicate significant differences between sites ($p < 0.05$).

Site (code)	No trees	No measured vessels	Vessel area (mm^2)	Minimum – maximum vessel diameter (μm)	Dh (μm)	Vessel density (No. mm^{-2})
Soto de la Remonta (RE)	5	195	0.037 ± 0.001b	100.98 – 284.90	250.12 ± 1.96b	14 ± 1a
Soto de Partinchas (PA)	5	195	0.030 ± 0.001a	95.45 – 249.70	188.97 ± 2.30a	19 ± 1b

3. Results

3.1. Structure and mortality in elm stands

The elm importance values were relatively high (greater than 0.10) in 5 out of the 13 study sites (Table 1). The highest basal area values of living elm trees were found in the well-preserved Murillo de las Limas (13.2 m^2 ha^{-1}, 30.5 % of total basal area), Soto de Partinchas (8.4 m^2 ha^{-1}, 13.3 %) and Soto de la Remonta (6.4 m^2 ha^{-1}, 11.4 %) sites, and corresponded to stem densities ranging between 600 and 750 stems ha^{-1}. At site level, the elm importance value increased as *P. alba* importance value did ($r_s = 0.80$, $p = 0.0006$) and as the river sinuosity decreased ($r_s = -0.58$, $p = 0.0439$).

On average, 64.1 ± 11.7 % (mean ± SE) of the total elm basal area and 33.7 ± 7.9 % of the total elm stem density corresponded to dead trees. In some sites, elm mortality was close to 50 % of the species basal area (well-preserved Soto de la Remonta and Soto de Partinchas sites), whereas in others it was close to 60 % (urban site "Iron bridge – left margin"; Fig. 2).

The fitted logit model (death probability = ($e^{(0.176\ dbh)} - 3.681$) / ($(1 + e^{(0.1767\ dbh)}) - 3.681$) had a likelihood function value of −80.54 and $p < 0.001$ (Fig. 3). The model showed that elm death probability was above 50 % for stem diameters > 21 cm.

3.2. Intra-annual growth patterns of elm trees

In the well-preserved Soto de Partinchas study site, elm growth peaked in April (2023) or May (2024) (Fig. 4). Cumulative radial growth differed between the two study sites, being more than two times higher in 2024 (2.4 mm) than in 2023 (0.7 mm). We found a higher tree water deficit in 2023 (0.55 mm), when it peaked in August, than in 2024 (0.1 mm), when it peaked in September. These differences were explained by the drier spring conditions observed in 2023 (Fig. S4).

3.3. Elm growth patterns and responses to climate, drought severity and river flow

Site mean growth rates ranged between 1.83 (well-preserved Soto de la Remonta site) and 4.53 mm (urban site "Iron bridge − left margin") (Table 2).

The first-order autocorrelation showed the lowest values in the urban

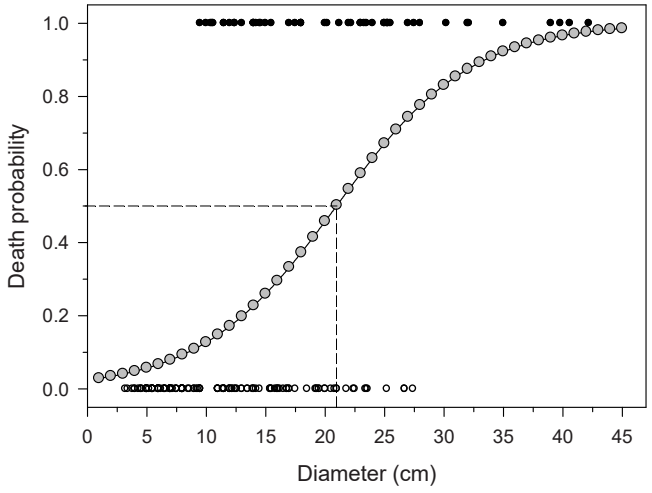

Fig. 3. Logit model (grey circles) of *Ulmus minor* death probability as a function of tree diameter at breast height (dbh). Data correspond to 180 trees sampled in the middle Ebro Basin riparian forests, which were classified as living (probability = 0, open white circles, n = 129) or dead (probability = 1, n = 51, closed black circles) individuals. Dashed lines show that the death probability above 50 % corresponds to elms with Dbh > 21 cm.

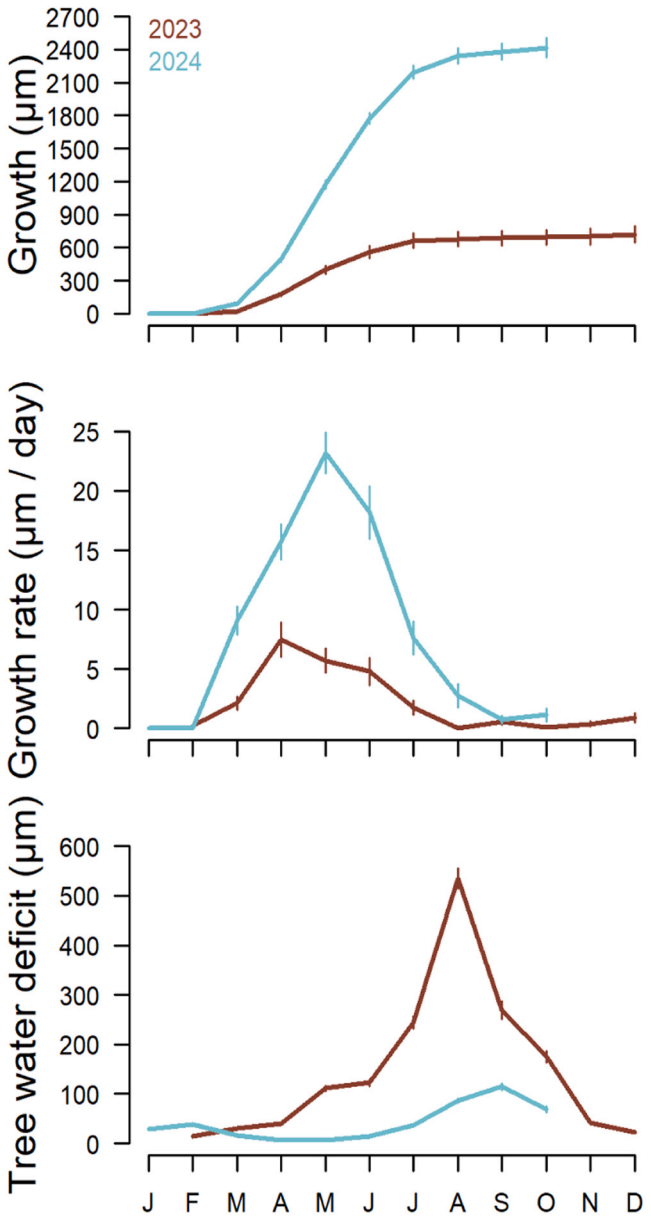

Fig. 4. Cumulative radial growth, growth rates and tree water deficit measured in 2023 and 2024 with point dendrometers in elm trees from the Soto de Partinchas study site. Values are means ± SE.

"Iron bridge" sites where fast-growing trees dominated and mortality peaked (Fig. 2). The mean sensitivity and rbar showed maximum values in the well-preserved Soto de Partinchas and Soto de la Remonta sites, respectively. The oldest living elms were found in the Murillo de Limas and Remonta sites and they were 83 and 81 years old, respectively. The oldest dated elm (90 years) was found in the first site, but it was recently dead.

According to correlations among site chronologies, those most strongly related (Soto de Partinchas, Iron bridge sites) were located near Zaragoza, followed by the Soto de la Duquesa (Table S1). The PCA biplot showed that the sites located near Tudela (Soto de la Remonta, Murillo de Limas) presented a slightly different growth variability with higher scores along the PC2 (Fig. S6). In the PCA biplot, the rings formed in 2012 and 2013 stood out as some of the narrowest and widest ones, respectively.

The high growth rate observed in 2013 indicated a very good recovery after the severe drought of 2012 (Fig. 5). This indicated that the

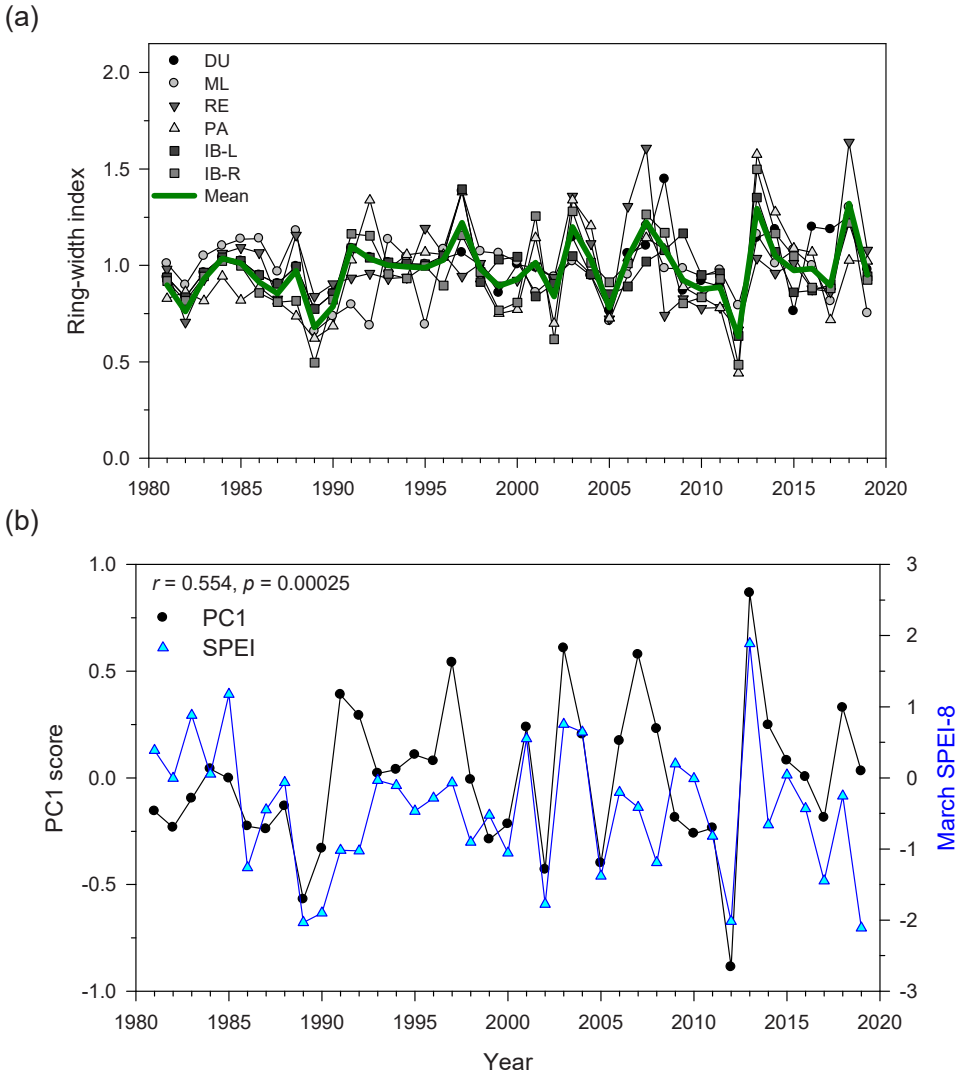

Fig. 5. (a) Growth variability in the sampled elm stands. The green line is the average of all sites' chronologies. (b) Positive relationship found between the PC1 scores and the 8-month March SPEI. See the correspondence between site code and name in Table 2.

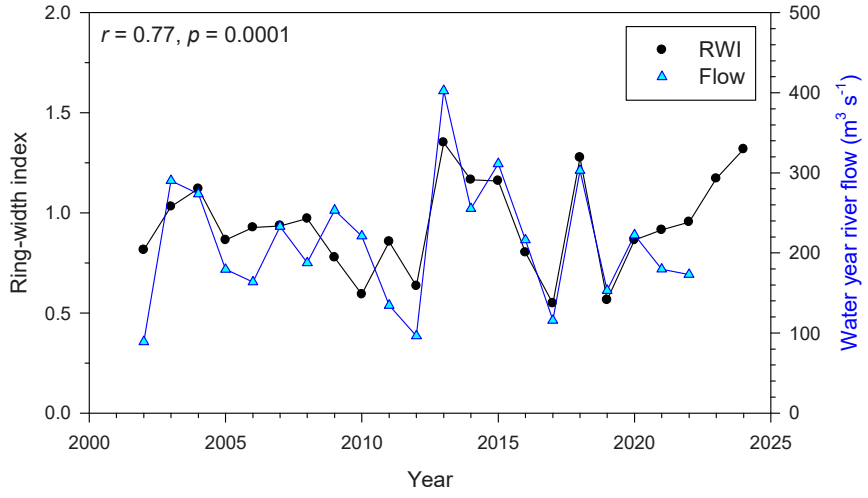

Fig. 6. Positive relationship found between water-year river flow (blue symbols, right *y* axis) and elm ring-width indices (RWI, black symbols) in the Soto de Partinchas site.

PC1 score was driven by drought severity. In fact, the PC1 scores were positively related to the 8-month March SPEI ($r = 0.554$, $p = 0.00025$), which encompassed the water balance from the previous summer to the current early spring. The PC2 scores were related to growth indices at the Soto de la Remonta site, where a low sinuosity index was also measured (Table 1).

In some sites, elm radial growth also depended on river flow. For instance, growth at the sites where the earlywood anatomy data were obtained positively responded to spring (Soto de la Remonta) and spring-summer river flow (Soto de Partinchas; Table S2). At the second site, a positive correlation between growth indices and water-year river flow ($r = 0.770$, $p = 0.0001$) was found (Fig. 6).

3.4. Earlywood anatomy of elm trees

Earlywood vessel area and Dh were higher in the elms from Soto de la Remonta than in those from Soto de Partinchas, whereas vessel density was lower (Table 3).

We found other associations between earlywood data and climate or river-flow variables. In the Soto de Partinchas, the ring area increased as

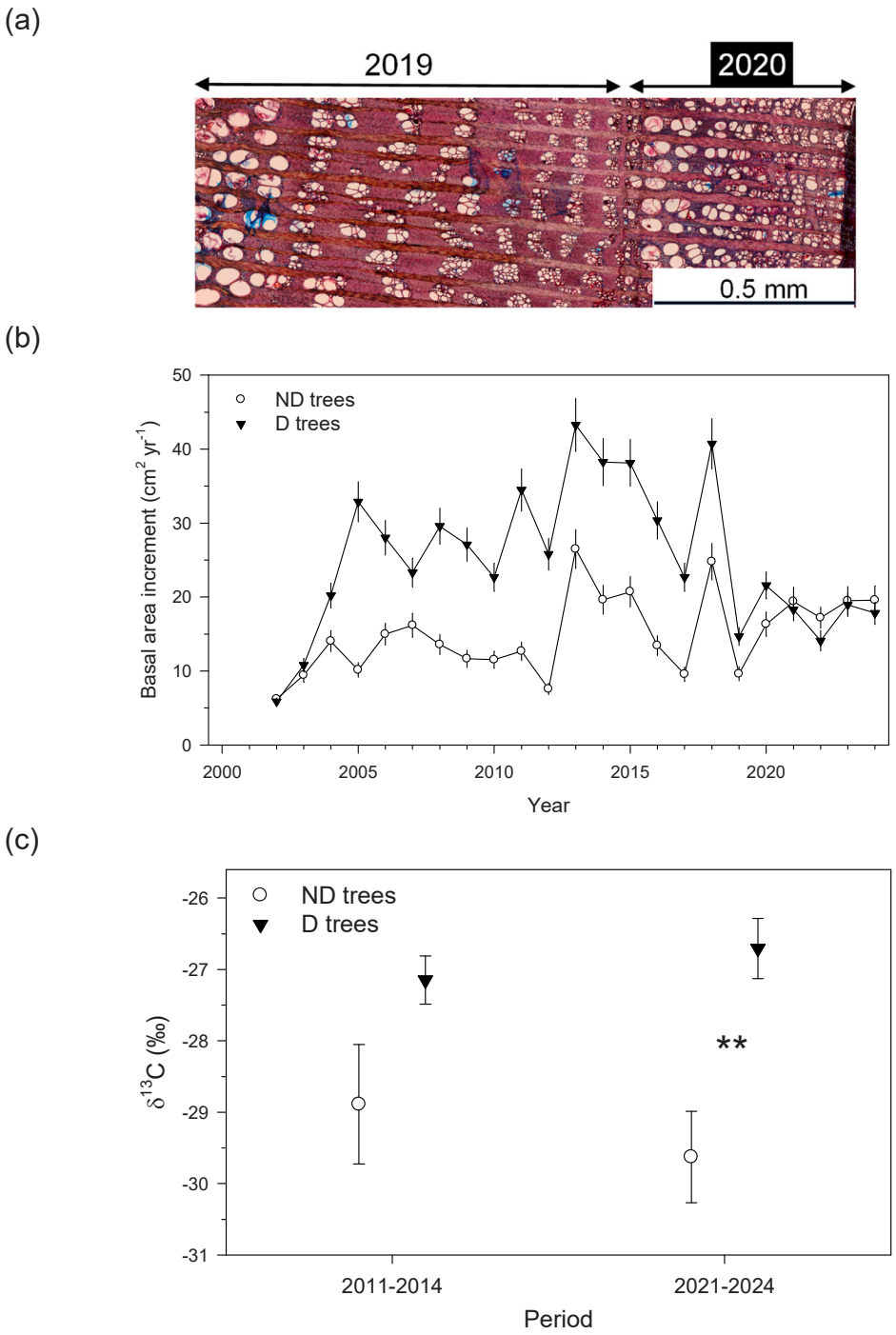

Fig. 7. (a) Wood cross-section of a DED-related dying tree showing reduced growth in the last tree ring. (b) Comparison of growth rates in non-declining (ND) and declining (D) trees. (c) Wood $\delta^{13}C$ values of ND and D trees corresponding to the periods 2011 −2014 and 2021 −2024. Wood $\delta^{13}C$ values of ND and D trees significantly differed in the last period (**$p < 0.01$). Values are means ± SE. All data correspond to elms sampled in the Iron bridge sites.

the March river discharge (Fig. S7) and February precipitation did (Fig. S8). At this site, the minimum earlywood diameter decreased as the previous December minimum temperature increased (Fig. S8). However, at the Soto de la Remonta, the minimum earlywood diameter decreased as the March minimum temperature or April precipitation increased (Fig. S9).

3.5. Growth and wood $\delta^{13}C$ in declining and non-declining elm trees

When comparing growth patterns of elms from the Soto de Partinchas and "Iron Bridge – left margin" sites, we detected an abrupt growth reduction during the 2012 drought and strong recovery in 2013, but recovery afterwards was better in the first site whereas death waves (2017, 2020, etc.) were common in the second site (Fig. S10). There, D trees grew more in the past than ND trees until the last four years when D trees showed higher wood $\delta^{13}C$ values than ND trees (-26.71 ‰ vs -29.63 ‰, $t = -4.21$, $p = 0.009$; Fig. 7).

4. Discussion

As hypothesized, we found widespread field elm mortality in the study region and a diameter threshold for tree death. Although we did not carry out any pathological analyses to test the DED presence, all visual symptoms of dying elm trees concurred with those of this disease (shedding and yellowing of leaves in summer −flagging, brown wilted leaves, branch dieback, brown staining in the sapwood, bark beetle galleries, etc.). We also found that elm growth was very sensitive to changes in soil moisture mediated by mid-term droughts that lasted from the previous summer to the early spring (hypothesis (ii)). This finding agrees with the observed periods of more active radial growth (April, May) and tree water deficit in late summer to early autumn (August, September). Therefore, this temporal window is critical for elm growth under Mediterranean conditions, whereas higher river flow levels in spring and summer also seem to be important for elm growth. A similar result was found for coexisting narrow-leaved ash trees (*F. angustifolia*) in the same sites (Rodríguez-González et al., 2021; Campelo et al., 2022; Camarero et al., 2023a). In contrast, warm winter-spring conditions lead to smaller earlywood vessel diameters, as has been observed in temperate and Mediterranean oaks (García-González and Eckstein, 2003, Alla and Camarero, 2012), which could restrict the stem hydraulic conductivity and spring growth.

The stand structure data showed widespread elm mortality and a higher abundance at sites with lower river sinuosity and higher *P. alba* abundance. This was partly unexpected because this is an obligate phreatophyte; however, in mature riparian forests elm is usually found in higher terraces located inland and coexisting with the facultative phreatophyte narrow-leaved ash (Ayerra, 1988). These results confirm what Camarero et al. (2023b) previously found: a historical disconnection between river dynamics and compositional changes of riparian forests. This is more evident in urban forests such as the Iron bridge site, where the loss of river sinuosity could reduce soil moisture levels in spring and aggravate drought stress, leading to decline in elm growth enhancing DED damage. These urban elm stands were characterized by high growth and mortality rates. Therefore, they should be specifically managed to reduce the DED spread and incidence of DED by creating more structurally diverse stands that mimic nearby forests showing lower DED-related elm mortality. For instance, urban sites (e.g., Iron bridge) could be managed to resemble sites subjected to more natural dynamics (e.g., Soto de la Duquesa, Soto de Partinchas). In addition, high elm mortality leads to abundant coarse woody debris and offers opportunities for other shade-intolerant woody species such as ivy. Such successional trajectories should be also better investigated.

We provide evidence that hotter spring droughts negatively impact the growth of field elm stands in the middle Ebro basin, as was found in other Mediterranean rivers, where the water shortage was intensified by hydrological and geomorphological changes affecting soil water depth (Stella et al., 2013). Several elm species also show a high dependence of radial growth on growing-season precipitation and river flow, and also present remarkable post-drought recovery. For instance, the growth of Siberian elm was constrained by water shortage from May to June, when the water deficit peaks across its native habitat in semi-arid Asian steppe sites (Babushkina et al., 2019). In temperate forests from North Eastern China, *Ulmus davidiana* Planch. showed a very good recovery after extreme droughts (Gong et al., 2024). In Illinois (USA), the radial growth of *Ulmus americana* L. positively responded to increased annual streamflow (Mitsch and Rust, 1984). The field elm shows strong and negative impacts of water shortage on radial growth, particularly in provenances susceptible to DED (Pita et al., 2018). Further research could explicitly analyse DED incidence or severity in elms subjected to different long-term drought severity or contrasting river-flow regimes to discern how this affects post-drought growth resilience.

Finally, we found that DED-infected trees showed higher wood $\delta^{13}C$ (enhanced iWUE) and their growth was drastically reduced (hypothesis (iii), indicating that DED amplifies drought stress and triggers growth decline prior to tree death. The $\delta^{13}C$ values measured in wood (−28.1 ‰, on average) were lower than those measured in elms from central Spain (−24.9 ‰; González-Muñoz et al., 2015), where conditions are warmer and drier than in the study sites of the middle Ebro basin. The improved iWUE could be an indirect effect of branch dieback and leaf shedding and wilting reducing water loss through leaves. Interestingly, declining trees showed higher growth rates in the past which could correspond to a prolific water-use strategy and the production of wider vessels leading to higher conductivity and making those trees more prone to DED-induced xylem blockage. In the case of elm seedlings, those clones most susceptible to DED showed the highest vessel lumen area and presented high growth rates (Pita et al., 2018). A similar pattern was found for fast-growing Scots pine (*Pinus sylvestris* L.) trees which were more predisposed to drought damage because they formed wider vessels and showed a profligate water use (Voltas et al., 2013).

5. Conclusions

Riparian forests are characterized by high productivity and fertile soils which make them vulnerable to agricultural use, but also to aggressive pathogens such as DED and others that are causing widespread mortality of several key tree species (elm, ash, alder). Our results suggest that fast-growing elm trees may be more prone to DED-induced damage, causing irreversible growth decline and increased iWUE. Elm radial growth was constrained by dry conditions from the previous summer to the current spring and by low river-flow levels, whereas earlywood vessel diameters decreased in response to winter-spring high temperatures. Consequently, changes in long-term soil moisture availability, driven by increasing temperatures or by hydrological alterations, can have a different impact on field elm growth and vitality. More diverse riparian forests with sufficient soil subjected to dynamic flooding regimes are required to preserve field elm populations. Managers should aim to preserve slow-growing stands or trees, which may be less susceptible to DED, by restoring river-forest interactions and promoting more diverse stands.

CRediT authorship contribution statement

Michele Colangelo: Writing – review & editing, Visualization, Validation, Software, Methodology, Investigation, Formal analysis, Data curation. **Antonio Gazol:** Writing – review & editing, Visualization, Validation, Supervision, Software, Methodology, Investigation, Funding acquisition, Formal analysis, Data curation. **Fernandez-Cortes Angel:** Writing – review & editing, Supervision, Resources, Methodology, Investigation, Formal analysis, Data curation. **J. Julio Camarero:** Writing – original draft, Visualization, Validation, Supervision, Software, Resources, Methodology, Investigation, Funding acquisition,

Formal analysis, Data curation, Conceptualization.

Declaration of Competing Interest

The authors declare that they have no known competing financial interests or personal relationships that could have appeared to influence the work reported in this paper.

Acknowledgements

This research was funded by the BBVA Foundation (SED-IBER project) and by the Science and Innovation Ministry projects PID2021–123675OB-C43 and TED2021–129770B-C21. We thank A. Sánchez-Miranda, P.M. Rodríguez-Gonzalez, R. Sánchez-Salguero and E. González de Andrés for their valuable help during field sampling.

Appendix A. Supporting information

Supplementary data associated with this article can be found in the online version at doi:10.1016/j.foreco.2025.122948.

Data availability

Data will be made available on request.

References

Alla, A.Q., Camarero, J.J., 2012. Contrasting responses of radial growth and wood anatomy to climate in a Mediterranean ring-porous oak: implications for its future persistence or why the variance matters more than the mean. Eur. J. For. Res. 131, 1537–1550.

Ayerra, E., 1988. Los sotos de la ribera Tudelana. Servicio de Medio Ambiente del Gobierno de Navarra, Pamplona, Spain.

Babushkina, E.A., Zhirnova, D.F., Belokopytova, L.V., Tychkov, I.I., Vaganov, E.A., Krutovsky, K.V., 2019. Response of four tree species to changing climate in a moisture-limited area of South Siberia. Forests 10, 999. https://doi.org/10.3390/f10110999.

Bertolasi, B., Leonarduzzi, C., Piotti, A., et al., 2015. A last stand in the Po valley: genetic structure and gene flow patterns in *Ulmus minor* and *U. pumila*. Ann. Bot. 115, 683–692. https://doi.org/10.1093/aob/mcu256.

Brasier, C.M., 1991. *Ophiostoma novo-ulmi* sp. nov., Causative Agent of Current Dutch Elm Disease Pandemics. Mycopathologia 115, 151–161.

Brasier, C.M., 2000. Intercontinental spread and continuing evolution of the Dutch elm disease pathogens. In: Dunn, C. (Ed.), The Elms: Breeding, Conservation and Disease Management. Kluwer, Dordrecht, pp. 61–72.

Briffa, K.R., Jones, P.D., 1990. Basic chronology statistics and assessment. In: Cook, E.R., Kairiukstis, L. (Eds.), Methods of Dendrochronology: Applications in the Environmental Sciences. Kluwer, Dordrecht, The Netherlands, pp. 137–152.

Bunn, A.G., 2008. A dendrochronology program library in R (dplR). Dendrochronologia 26, 115–124. https://doi.org/10.1016/j.dendro.2008.01.002.

Bunn, A.G., 2010. Statistical and visual crossdating in R using the dplR library. Dendrochronologia 28, 251–258. https://doi.org/10.1016/j.dendro.2009.12.001.

Bunn, A.G., Korpela, M., Biondi, F., Campelo, F., Mérian, P., Qeadan, F., Zang, C., 2024. dplR: Dendrochronology Program Library in R. R package version 1.7.7, ⟨https://CRAN.R-project.org/package=dplR⟩.

Camarero, J.J., Colangelo, M., Rodríguez-González, P.M., Sánchez-Miranda, A., Sánchez-Salguero, R., Campelo, F., Rita, A., Ripullone, F., 2021. Wood anatomy and tree growth covary in riparian ash forests along climatic and ecological gradients. Dendrochronologia 70, 125891.

Camarero, J.J., Colangelo, M., Rodríguez-González, P.M., 2023a. Tree growth, wood anatomy and carbon and oxygen isotopes responses to drought in Mediterranean riparian forests. For. Ecol. Manag. 529, 120710.

Camarero, J.J., Colangelo, M., Rodríguez-Gonzalez, P.M., 2023b. Historical disconnection from floodplain alters riparian forest composition, tree growth and deadwood amount. Sci. Total Environ. 896, 165266.

Campelo, F., Sánchez-Salguero, R., Rodríguez-González, P.M., Colangelo, M., Sánchez-Miranda, A., Rita, A., Ripullone, F., Camarero, J.J., 2022. Growth adjustments to climate permit ash riparian forests to face summer droughts in southern Europe. Dendrochronologia 76, 126013.

Caudullo, G., De Rigo, D., 2016. Ulmus –elms in Europe: distribution, habitat, usage and threats. In: San-Miguel-Ayanz, J., De Rigo, D., Caudullo, G., Durrant, T., Mauri, A. (Eds.), European Atlas Forest Tree Species. EU, Luxembourg, pp. 186–188.

Colangelo, M., Camarero, J.J., Ripullone, F., Gazol, A., Sánchez-Salguero, R., Oliva, J., Redondo, M.A., 2018. Drought decreases growth and increases mortality of coexisting native and introduced tree species in a temperate floodplain forest. Forests 9, 1–17.

Cornes, R., van der Schrier, G., van den Besselaar, E.J.M., Jones, P.D., 2018. An ensemble version of the E-OBS temperature and precipitation datasets. J. Geophys. Res. Atmos. 123, 9391–9409. https://doi.org/10.1029/2017JD028200.

Cottam, G., Curtis, J.T., 1956. The use of distance measure in phytosociological sampling. Ecology 37, 451–460.

Dufour, S., Piégay, H., 2008. Geomorphological controls of Fraxinus excelsior growth and regeneration in floodplain forests. Ecology 89, 205–215.

Ellmore, G.S., Ewers, F.W., 1985. Hydraulic conductivity in trunk xylem of Elm, *Ulmus americana*. IAWA Bull. 4, 303–307.

Fritts, H., 1976. Tree Rings and Climate. Academic Press, London.

Frutos, L.M., Ollero, A., Sánchez-Fabre, M., 2004. Caracterización del Ebro y su cuenca y variaciones en su comportamiento hidrológico. In: Gil Olcina, A. (Ed.), Alteración de los regímenes fluviales peninsulares, edited by. Fundación Cajamurcia, Murcia, Spain, pp. 233–280.

García-González, I., Eckstein, D., 2003. Climatic signal of earlywood vessels of oak on a maritime site. Tree Physiol. 23, 497–504.

Gärtner, H., Nievergelt, D., 2010. The core-microtome, a new tool for surface preparation on cores and time series analysis of varying cell parameters. Dendrochronologia 28, 85–92.

Gong, X., Yuan, D., Zhu, L., Li, Z., Wang, X., 2024. Long-term changes in radial growth of seven tree species in the mixed broadleaf-Korean pine forest in Northeast China: are deciduous trees favored by climate change? J. For. Res. 35, 70. https://doi.org/10.1007/s11676-024-01725-7.

González Muñoz, N., Linares, J.C., Castro-Díez, P., Sass-Klaassen, U., 2015. Contrasting secondary growth and water use efficiency patterns in native and exotic trees co-occurring in inner Spain riparian forests. For. Syst. 24, e017. https://doi.org/10.5424/fs/2015241-06586.

Gurnell, A.M., Scott, S.J., England, J., Gurnell, D., Jeffries, R., Shuker, L., Wharton, G., 2020. Assessing river condition: a multiscale approach designed for operational application in the context of biodiversity net gain. River Res. Appl. 36, 1559–1578. https://doi.org/10.1002/rra.3673.

Havrdová, A., Douda, J., Doudová, J., 2023. Threats, biodiversity drivers and restoration in temperate floodplain forests related to spatial scales. Sci. Total Environ. 854, 158743. https://doi.org/10.1016/j.scitotenv.2022.158743.

Holmes, R.L., 1983. Computer-assisted quality control in tree-ring dating and measurement. TreeRing Bull. 43, 69–78.

Janssen, P., Stella, J.C., Räpple, B., et al., 2021. Long-term river management legacies strongly alter riparian forest attributes and constrain restoration strategies along a large, multi-use river. J. Environ. Manag. 279, 111630.

Kibler, C.L., Schmidt, E.C., Roberts, D.A., Stella, J.C., Kui, L., Lambert, A.M., Singer, M. B., 2021. A brown wave of riparian woodland mortality following groundwater declines during the 2012–2019 California drought. Environ. Res. Lett. 16, 084030.

Knüsel, S., Peters, R.L., Haeni, M., Wilhelm, M., Zweifel, R., 2021. Processing and extraction of seasonal tree physiological parameters from stem radius time series. Forests 12, 765. https://doi.org/10.3390/f12060765.

Larsson, L.A., Larsson, P.O., 2018. CDendro and CooRecorder (v. 9.3.1); Cybis Elektronik and Data AB. Saltsjöbaden, Sweden.

Martín, J.A., Domínguez, J., Solla, A., et al., 2023. Complexities underlying the breeding and deployment of Dutch elm disease resistant elms. N. For. 54, 661–696. https://doi.org/10.1007/s11056-021-09865-y.

Martínez-Arias, C., Sobrino-Plata, J., Macaya-Sanz, D., et al., 2020. Changes in plant function and root mycobiome caused by flood and drought in a riparian tree. Tree Physiol. 40, 886–903. https://doi.org/10.1093/treephys/tpaa031.

Mitsch, W.J., Rust, W.G., 1984. Tree growth responses to flooding in a Bottomland Forest in Northeastern Illinois. For. Sci. 30, 499–510. https://doi.org/10.1093/forestscience/30.2.499.

Mittempergher, L., 1989. Il declino dell'olmo: da latifoglia nobile a cespuglio. Ann. Accad. Ital. Sci. For. 38, 585–609.

Mittempergher, L., Santini, A., 2004. The history of elm breeding. Invest. óN. Agrar. Sist. Y. Recur. For. 13, 161–177.

Moran, M.E., Aparecido, L.M.T., Koepke, D.F., Cooper, H.F., Doughty, C.E., Gehring, C. A., Throop, H.L., Whitham, T.G., Allan, G.J., Hultine, K.R., 2023. Limits of thermal and hydrological tolerance in a foundation tree species (*Populus fremontii*) in the desert southwestern United States. N. Phytol. 240, 2298–2311. https://doi.org/10.1111/nph.19247.

Mueller, J.E., 1968. An introduction to the hydraulic and topographic sinuosity indexes. Ann. Assoc. Am. Geogr. 58, 371–385.

Muller-Dombois, D., Ellenberg, H., 1974. Aims and Methods of Vegetation Ecology. John Wiley and Sons.

Oksanen, J., Simpson, G., Blanchet, F., Kindt, R., Legendre, P. et al. 2025. vegan: Community Ecology Package. R package version 2.7-0, ⟨https://github.com/vegandevs/vegan⟩, ⟨https://vegandevs.github.io/vegan/⟩.

Ollero, A., 1990. Espacios naturales de ribera en el municipio de Zaragoza. Geographicalia 27, 121–136.

Ollero, A., 2007. Channel adjustments, floodplain changes and riparian ecosystems of the middle Ebro River: assessment and management. Int. J. Water Resour. D. 23, 73–90.

Pita, P., Rodríguez-Calcerrada, J., Medel, D., Gil, L., 2018. Further insights into the components of resistance to *Ophiostoma novo-ulmi* in *Ulmus minor*: hydraulic conductance, stomatal sensitivity and bark dehydration. Tree Physiol. 38, 252–262.

R Development Core Team, 2024. R: A Language and Environment for Statistical Computing.

Rodríguez-González, P.M., Stella, J.C., Campelo, F., Ferreira, M.T., Albuquerque, A., 2010. Subsidy or stress? Tree structure and growth in wetland forests along a hydrological gradient in Southern Europe. For. Ecol. Manag 259, 2015–2025. https://doi.org/10.1016/j.foreco.2010.02.012.

Rodríguez-González, P.M., Colangelo, M., Sanchez-Miranda, A., Sánchez-Salguero, R., Campelo, F., Rita, A., Gomes Marques, I., Albuquerque, A., Ripullone, F., Camarero, J.J., 2021. Climate, drought and hydrology drive narrow-leaved ash growth dynamics in southern European riparian forests. For. Ecol. Manag 490, 119128. https://doi.org/10.1016/j.foreco.2021.119128.

Schmucker, J., Uhl, E., Schmied, G., Pretzsch, H., 2023. Growth and drought reaction of European hornbeam, European white elm, field maple and wild service tree. Trees Struct. Funct. 37, 1515–1536. https://doi.org/10.1007/s00468-023-02441-1.

Schneider, C.A., Rasband, W.S., Eliceiri, K.W., 2012. NIH Image to ImageJ, 25 years of image analysis. Nat. Methods 9, 671–675.

Solla, A., Martín, J.A., Corral, P., Gil, L., 2005. Seasonal changes in wood formation of *Ulmus pumila* and *U. minor* and its relation with Dutch elm disease. N. Phytol. 166, 1025–1034.

Sperry, J.S., Nichols, K.L., Sullivan, J.E.M., Eastlack, S.E., 1994. Xylem embolism in ring-porous, diffuse-porous, and coniferous trees of northern Utah and interior Alaska. Ecology 75, 1736–1752.

Stella, J.C., Bendix, J., 2019. Multiple stressors in riparian ecosystems. Multiple Stressors in River Ecosystems. Elsevier, pp. 81–110.

Stella, J.C., Riddle, J., Piégay, H., Gagnage, M., Trémélo, M.-L., 2013. Climate and local geomorphic interactions drive patterns of riparian forest decline along a Mediterranean Basin river. Geomorphology 202, 101–114.

Stromberg, J.C., Tiller, R., Richter, B., 1996. Effects of groundwater decline on riparian vegetation of semiarid regions: the San Pedro, Arizona. Ecol. Appl. 6, 113–131.

Tulik, M., Grochowina, A., Jura-Morawiec, J., Bijak, S., 2020. Groundwater Level Fluctuations Affect the Mortality of Black Alder (*Alnus glutinosa* Gaertn.). Forests 11, 134.

Valor, T., Camprodon, J., Buscarini, S., Casals, P., 2020. Drought-induced dieback of riparian black alder as revealed by tree rings and oxygen isotopes. For. Ecol. Manag 478, 118500.

Vicente-Serrano, S.M., Beguería, S., López-Moreno, J.I., 2010. A multiscalar drought index sensitive to global warming: the standardized precipitation evapotranspiration index. J. Clim. 23, 1696–1718.

Voltas, J., Camarero, J.J., Carulla, D., Aguilera, M., Oriz, A., Ferrio, J.P., 2013. A retrospective, dual-isotope approach reveals individual predispositions to winter-drought induced tree dieback in the southernmost distribution limit of Scots pine. Plant Cell Environ. 36, 1435–1448.

Williams, C.A., Cooper, D.J., 2005. Mechanisms of riparian cottonwood decline along regulated rivers. Ecosystems 8, 382–395.

Zang, C., Biondi, F., 2015. treeclim: an R package for the numerical calibration of proxy-climate relationships. Ecography 38, 431–436.

Zweifel, R., Haeni, M., Buchmann, N., Eugster, W., 2016. Are trees able to grow in periods of stem shrinkage? N. Phytol. 211, 839–849. https://doi.org/10.1111/nph.13995.